DNS OF HYPERSONIC BOUNDARY LAYER STABILITY AND TRANSITION USING HIGH-ORDER NONUNIFORM-GRID SCHEMES

XIAOLIN ZHONG
Mechanical and Aerospace Engineering Department
University of California, Los Angeles, CA 90095

Abstract

High-order schemes are necessary for the DNS of stability and transition of hypersonic boundary layers because lower-order schemes do not have a sufficient accuracy level to compute small flow details. Currently, the main limiting factor in the application of high-order schemes is the numerical instability of high-order boundary closure schemes. In a previous AIAA paper (2001-0437), we presented a family of high-order nonuniform-grid finite-difference schemes with stable boundary closures for multi-dimensional flow simulations. In this paper, the high-order nonuniform-grid schemes (up to 11th order) are applied to the numerical simulation of the receptivity of hypersonic boundary layers to freestream disturbances over a blunt leading edge. The stability and numerical accuracy of the new high-order nonuniform-grid schemes are evaluated for computing the nonlinear 2-D Navier-Stokes equations for hypersonic flow simulations.

1. Introduction

The prediction of laminar-turbulent transition in hypersonic boundary layers is a critical part of the aerodynamic design and control of hypersonic vehicles. The transition process is a result of the nonlinear response of laminar boundary layers to forcing disturbances, which can originate from many difference sources including free stream disturbances, surface roughness and vibrations. In an environment with weak initial disturbances, the path to transition consists of three stages: 1) receptivity, 2) linear eigenmode growth or transient growth, and 3) nonlinear breakdown to turbulence. Due to the complexity of transient hypersonic flow fields including the instability and receptivity process, an effective approach to studying hypersonic boundary

layer stability and receptivity is the direct numerical simulation of the full Navier-Stokes equations. In (1) and (2), we presented and validated a new fifth-order upwind finite difference shock fitting method for the direct numerical simulation of hypersonic flows with a strong bow shock. The use of the high-order shock-fitting scheme makes it possible to obtain highly accurate mean flow and unsteady solutions, which are free of spurious numerical oscillations behind the bow shock. The method has been subsequently validated and applied to numerical studies of receptivity and stability of many two and three-dimensional hypersonic boundary-layer flows.

The application of high-order finite-difference schemes have recently received much attention in many areas of flow simulations, including the direct numerical simulation (DNS) of transitional and turbulent flows[2; 3; 4; 5], and other areas. High-order schemes are necessary in such flow simulations because lower-order schemes do not have sufficient accuracy to compute small flow details. Currently, most high-order finite-difference schemes are derived on uniformly spaced grid points. The schemes are applied to a nonuniform grid by a coordinate transform from the nonuniform physical domain to a uniform computational domain. The main limiting factor in the application of high-order schemes is the numerical instability of high-order boundary closure schemes[6; 7]. For example, Carpenter et al.[6] showed that for a sixth-order inner compact scheme, only a third-order boundary scheme can be used without introducing instability. Consequently, the order of accuracy of numerical schemes used in most practical DNS studies is often limited to 6th-order or lower in the interior and 4th-order or lower on the boundary closure schemes because of the numerical instability of boundary closure schemes. It is necessary to overcome the instability of boundary closure schemes in order to have wide applications of arbitrarily high-order schemes to practical multi-dimensional flow simulations.

In Ref. (8), we showed that it is possible to use high-order (11th or higher order) explicit and compact finite difference schemes with stable boundary closures for high accurate numerical simulation of incompressible and compressible flows. We proposed a simple and effective way to overcome the instability in arbitrarily high-order finite difference schemes with boundary closure schemes. It was shown that the numerical instability of high-order boundary schemes is a result of the use of uniform computational grids in applying high-order schemes. An effective way to overcome the instability for arbitrary high-order finite difference schemes with boundary closure schemes is to use the high-order schemes directly in a nonuniform stretched grid without coordinate transformation. The coefficients of the high-order schemes are determined based on polynomial interpolation in the physical nonuniform grids. The amount of grid stretching is determined to maintain the stability of the overall schemes. The new high-order (up to 12-th

order) schemes have been analyzed and tested in computing a linear wave equation with oscillatory boundary conditions. It was found the high-order schemes are stable and produce a much higher degree of accuracy than lower order schemes. It is not clear, however, if the accuracy and stability of the high-order non-uniform grid schemes can be maintained when they are applied to simulation of complex multidimensional flow fields using the nonlinear Navier-Stokes equations. The purpose of this paper is to apply the new high-order schemes to the DNS of the receptivity and stability of hypersonic boundary layer flows over a 2-D blunt body. The stability and numerical accuracy are quantitatively evaluated based on the numerical solutions.

2. Governing Equations

The governing equations for DNS of hypersonic flows are the unsteady two or three-dimensional Navier-Stokes equations in the following conservation-law form (for 2-D cases):

$$\frac{\partial U^*}{\partial t^*} + \frac{\partial F^*{}_j}{\partial x_j^*} + \frac{\partial F^*{}_{vj}}{\partial x_j^*} = 0 \tag{1}$$

where superscript "$*$" represents dimensional variables. The vector of the conservative flow variables is $U^* = \{\rho^*,\ \rho^* u_1^*,\ \rho^* u_2^*,\ e^*\}$ The gas is assumed to be thermally and calorically perfect. The viscosity and heat conductivity coefficients are calculated using Sutherland's law together with the assumption of a constant Prandtl number.

3. Coordinate Mapping in Shock Fitting Simulations

Numerical simulations for hypersonic flows over a blunt leading edge are carried out using the high-order nonuniform-grid schemes presented in (8) with a shock fitting treatment for the bow shock. The unsteady bow shock shape and shock oscillations are calculated as part of the computational solution. The high-order nonuniform grid schemes are applied to the governing equations using a coordinate transformation. The spatially discretized equations are advanced in time using a low-storage Runge-Kutta scheme of up to third order.

The computational domain for a shock-fitting method used in computating steady and unsteady 2-D viscous hypersonic flow over blunt bodies is shown in Fig. 1. The governing equations are solved in a general curvilinear coordinates $(\xi,\ \eta,\ \tau)$ along body fitted grid lines. The computational domain in (x, y) between the bow shock and the body is transformed into a square domain in $(\xi, \eta) \in [-1, 1] \times [-1, 1]$. The governing equations (1)

are transformed into the computational domain (ξ, η, τ) resulting in:

$$\frac{1}{J}\frac{\partial U}{\partial \tau} + \frac{\partial E'}{\partial \xi} + \frac{\partial F'}{\partial \eta} + + \frac{\partial E'_v}{\partial \xi} + \frac{\partial F'_v}{\partial \eta} + U\frac{\partial(\frac{1}{J})}{\partial \tau} = \frac{W}{J} \tag{2}$$

where J is the Jacobian of the coordinate transformation.

For viscous flow simulations, the physical computational domain between the bow shock and the body (Fig. 1) is mapped to a square in two steps: 1) (x, y, t) to (X, Y, τ), and 2) (X, Y, τ) to (ξ, η, τ), following Kopriva[9]. First, the physical space is mapped to a square by the follow relation:

$$X = \frac{2s(x,y)}{S} - 1 \quad Y = \frac{2h(x,y)}{H(x,y,t)} - 1 \tag{3}$$

where s is the local surface length, S is total surface length in the computational domain, h is the local normal distance of point (x, y) to the body surface, and H is the local shock height. For unsteady flow, $H(x, y, t)$ is a function of time because of the shock motion. This transformation maps the physical space to a square $(X, Y) \in [-1, 1] \times [-1, 1]$. Second, the (X, Y) space is mapped to a square in (ξ, η) space in order to introduce more grid points near the wall to resolve the boundary layer structure better. A hyperbolic tangent stretching[9] is used in the wall-normal direction as follows:

$$Y = 2\frac{[1 - \tanh(\sigma)]^{\frac{\eta+1}{2}}}{1 - \tanh(\sigma^{\frac{\eta+1}{2}})} - 1 \tag{4}$$

where σ is the stretching parameter. The value of σ is chosen to be 0.75 in this paper. This combined transformation maps the physical space in (x, y) to a square space in $(\xi, \eta) \in [-1, 1] \times [-1, 1]$.

4. Interior High-Order Schemes with Stable Boundary Closure

The governing equations (2) in (ξ, η) space are discretized using the high-order nonuniform-grid finite difference schemes[8] in the square computational domain. In this paper, the grid spacing in the (ξ, η) space is given by the following stretching function[10]:

$$\xi_i = \frac{\sin^{-1}(-\alpha \cos(\pi i/N))}{\sin^{-1}\alpha} \quad \eta_j = \frac{\sin^{-1}(-\alpha \cos(\pi j/M))}{\sin^{-1}\alpha} \tag{5}$$

where the parameter α is used to change the stretching of the grid points, i and j are grid index numbers. The high-order nonuniform-grid scheme

applies a finite difference approximation directly to the grid points in the (ξ, η) space. The coefficients are derived from a Lagrange polynomial interpolation. For the case of an N-point grid stencil with a distribution of grid points with coordinates ξ_i, the $N-1$ degree interpolation polynomial is:

$$P_n(\xi) = \sum_{j=1}^{N} l_j(\xi)\, u_j \tag{6}$$

where u_j is the variables at the node points, and

$$l_j(\xi) = \prod_{l=1, l\neq j}^{n} (\xi - \xi_l) \;/\; \prod_{l=1, l\neq j}^{n} (\xi_j - \xi_l) \tag{7}$$

The derivative at a grid point ξ_i can be calculated by differentiating the above polynomial as: $u_i' = \sum_{j=1}^{N} b_{i,j}\, u_j$, where the coefficients $b_{i,j}$ in the derivatives are different for different grid points with index i. Hence, once the ξ_i locations of the stencil are known the coefficients for the finite difference formulas for a high-order scheme in a nonuniform grid can be calculated explicitly using the above formulas. The coefficients at the boundary closure scheme are derived using the same formula by specifying one-sided grid stencils. The derivatives at all grid points, including the interior and boundary points, can be combined into the following vector formula: $\boldsymbol{u}' = \boldsymbol{A}\boldsymbol{u}$, where $\boldsymbol{u}$ is a vector of variables and $\boldsymbol{A}$ is a banded coefficients matrix, which can be computed once and for all at the beginning of a calculation.

4.1. BOUNDARY CONDITIONS

The boundary condition at the bow shock is computed by a shock fitting method described in (2). On the wall, the physical non-slip condition for velocities ($u = v = 0$), and isothermal ($T = T_w$) or adiabatic condition are used. A characteristic equation is used to compute pressure on the wall. For flow conditions at the symmetrical center line, the conditions $v = 0$ and zero gradient for all other variables are used. For exit conditions, a simple extrapolation condition is used because the flow is supersonic outside the boundary layer.

5. Receptivity of Mach 15 Flow Over A Parabola

We apply the new high-order nonuniform grid schemes to compute the receptivity process of Mach 15 flows over a parabolic blunt leading edge. The receptivity mechanism provides important initial conditions of amplitude, frequency, and phase of instability waves in the boundary layers. The same

test case has been studied by Zhong[11] using a fifth-order shock fitting scheme. The receptivity problem is an ideal case to test the stability and accuracy of the new schemes because it involves both steady and unsteady flow simulation in a viscous hypersonic flow field. The unsteady flow field contains complex interactions between a number of waves of different length scales.

Specifically, the receptivity of a two-dimensional boundary layer to free stream acoustic waves in hypersonic flow past a parabolic leading edge at zero angle of attack is considered. The free stream disturbances are assumed to be weak monochromatic planar acoustic waves with wave fronts normal to the center line of the body. The flow is characterized by a free stream Mach number M_∞ and a Reynolds number Re_∞. The forcing frequency of the free stream acoustic wave is represented by a dimensionless frequency F defined as $F = 10^6 \frac{\omega^* \nu^*}{U_\infty^{*2}}$. We can also define a Strouhal number S using the nose radius by $S = \frac{\omega^* r^*}{U_\infty^*}$.

The flow conditions of the current computational case are as follows. $M_\infty = 15$, $T_\infty^* = 192.989\ K$, $p_\infty^* = 10.3\ Pa$, $\gamma = 1.4$, $Pr = 0.72$, $R^* = 286.94\ Nm/kgK$, $Re_\infty = 6026.6$, $T_w^* = 1000K$, $r^* = 0.0125\ m$, $d^* = 0.1\ m$, and $\epsilon = 5 \times 10^{-4}$ to 10^{-1}. The nondimensional frequency is $k_\infty = 15$, and $F = 2655$, $S = 2$. Two sets of grids are used to compute both steady and unsteady flow solutions of the full Navier-Stokes equations: a coarse 31×51 grid and a finer 51×91 grid. The computational grid of 31×51 is shown in Fig. 1. For each grid, the flow solutions are simulated using a nonuniform grid scheme of different orders. Specifically, the orders are 1st, 3rd, 5th, 7th, 9th, and 11th order. The grid stretching parameter α in Eq. (5) is 0.6, which has been found to be stable for the various order schemes computed.

5.1. STEADY BASE FLOW SOLUTIONS

The steady base flow solutions of the Navier-Stokes equations for the Mach 15 flow over the blunt leading edge are obtained first by advancing the solutions to a steady state without freestream perturbations. The physical characteristics of the solutions of this flow problem have been discussed in detail in (2). The main focus of this paper is to evaluate the numerical stability and accuracy of high-order nonuniform grid schemes at different orders and different grid resolutions.

Figure 2 shows the Mach number contours and velocity vectors for steady base flow solutions using the 11th-order nonuniform-grid scheme. The results computed by the 11th-order scheme are very smooth for this relatively coarse grid. Figure 3 shows five sets of pressure contours for steady base flow solutions using five nonuniform-grid schemes of the 1st, 3rd, 5th, 9th, and 11th order using the same 31×51 grid. The first order scheme

produces very large errors. The accuracy improves substantially by the use of the third order scheme. As the order increases further, the accuracy improves further and the numerical solution approaches the exact solution. Since there is no analytical solution available, we evaluate the numerical accuracy by comparing the present solutions with those of an 11th order scheme using a finer 51×91 grid. Figure 4 shows such accuracy evaluation for the surface distribution of vorticity using nonuniform-grid schemes of different orders. The lower figure shows the comparison near the minimum vorticity point. Again the figure shows the improvement of numerical accuracy as the order of the method increases. The 11th-order scheme using the coarse grid is very close to the results of fine grid of the same order. Similar trends in the numerical accuracy of the results are also shown in the pressure and surface heating rates distribution (Figs. 5 and 6).

Figures 7 and 8 show a quantitative assessment of the numerical accuracy of the schemes of different orders by plotting the relative errors of pressure and heating rates at the stagnation point. For a fixed grid resolution, the numerical accuracy of the schemes improves as the order of the schemes increases. The improvement is dramatic when the order is low. As the order increases, the improvement in accuracy becomes smaller. At very high-order, there is very little improvement in accuracy by increasing the order further, because it has reached the limit of the grid resolution. When a finer grid is used, the high-order schemes lead to further improvement of accuracy. Therefore, the accuracy of high-order schemes can be improved substantially by increasing the order of the schemes, but for a given grid resolution there is a limiting order of the schemes, beyond which the accuracy of the solutions can not be improved further unless the grid is further refined. For the current 2-D Navier-Stokes equations over a blunt body, the limiting order for the 31×51 grid is about 5th order, while the limit for the finer 51×91 grid is 9th order.

Overall, the stead-flow results show that the high-order nonuniform grid schemes are stable for very high-order (up to 11th order)schemes. Such high order solutions are not possible using a conventional uniform grid scheme because of numerical instability. The high-order nonuniform-grid schemes can produce highly accurate numerical solutions.

5.2. UNSTEADY FLOW SOLUTIONS

Having obtained the steady solution, the receptivity of the hypersonic boundary-layer in the Mach 15 flow over the parabola is studied by numerical simulation using the high-order schemes. The high-order nonuniform-grid schemes are used to compute the unsteady solutions induced by freestream acoustic waves. The forcing waves induce boundary layer waves inside the

boundary layers. The unsteady calculations are carried out until the solutions reach a periodic state in time. Temporal Fourier analysis is carried out on local perturbations of unsteady flow variables after a time periodic state has been reached. The Fourier transform for the real disturbance functions lead to:

$$q'(x,y,t) = \Re\{\sum_{n=0}^{N} |q_n(x,y)|\ e^{i[-n\omega_0 t+\phi_n(x,y)]}\} \tag{8}$$

where $n\omega_0$ is the frequency of the n-th wave mode, $q'(x,y,t)$ represents any perturbation variables. The boundary layer waves contain the fundamental wave mode, which has the same frequency F as the forcing acoustic waves. At the same time, due to the nonlinear interaction, the wave field also contains higher harmonics of the fundamental frequency, nF, where $n = 0$ represents mean distortion, $n = 1$ represents the fundamental mode, $n = 2$ represents the second harmonics of two times the fundamental frequency, etc. The higher harmonics have smaller wave lengths and orders of magnitude smaller amplitudes. For example, the wavelength of $n = 2$ mode is about half of that of the $n = 1$ fundamental mdoe.

The results presented here are those for the case of freestream frequency of $F = 2655$ and nondimensional freestream forcing wave amplitude of $\epsilon = 0.001$. The unsteady solutions are computed by the new nonuniform grid schemes of different orders. Figure 9 shows the instantaneous pressure and temperature perturbation contours. The solution is obtained by the 9th order scheme using a 51×91 grid. The results show a very smooth wave solution. In response to the perturbations of the forcing waves in the freestream, the unsteady flow field produces boundary layer wave modes of fundamental frequencies and their harmonics. In the present case, the higher harmonics are several orders of magnitudes weaker than the fundamental modes. Figure 10 shows the Fourier harmonics of the induced wave. It shows the Fourier amplitudes of pressure perturbation and their real parts along the parabola surface. The solution is obtained by the 7th order schemes using a 51×91 grid. In the figure, $n = 0, 1, 2, 3$, corresponds to mean flow distortion, fundamental mode, second harmonic, and third harmonic. The figures show that the high-order schemes are able to capture these modes with a relatively coarse grid. Notice that there are about 27, 18, and 9 grid points per period for the first ($n = 1$), the second ($n = 2$), and third harmonic ($n = 3$), respectively. The amplitudes of these three harmonics are in the order of 10^1, 10^{-1}, and 10^{-3} for the first, second, and third harmonics. The figures show that the 7th-order scheme captures all these modes well.

The results of wave harmonics obtained by different order schemes of the same grid are compared in Figs. 11 to 13. The results shows that the funda-

mental mode is captured very well by all three schemes of 5th, 7th, and 9th order. For second harmonics ($n = 2$), however, the 5th-order scheme is not as accurate, while the 7th and 9th order produce almost the same results. Similarly, the 5th-order scheme under predicts the mean flow distortion ($n = 0$ mode) caused by nonlinear wave interaction. Therefore, the 9th-order scheme produces more accurate results than the 5th-order scheme for the transient flow field when the length scale is small for the high harmonics and the mean flow distortion due to nonlinear interactions.

Similar to the steady solution case, it is necessary to have suffucient grid resolution for the flow length scale in order to have good accuracy. The corresponding unsteady flow have also been computed by using a relatively coarse 31×51 grid. Figure 14 shows the Fourier amplitudes of pressure perturbation along the parabola surface for the same case. The solution is obtained by the 9th order scheme using a 31×51 grid. The results show that the high-order schemes capture the fundamental mode very well, but cannot capture the higher harmonics accurately because of the coarser grid.

6. Conclusion

The high-order nonuniform grid schemes have been applied to 2-D hypersonic flow simulations using the nonlinear Navier-Stokes equations. Stable numerical solutions have been obtained for the receptivity of Mach 15 flow over a parabola. The accuracy of both steady and unsteady solutions obtained by using different orders of the schemes and different grid resolutions have been evaluated. The results show the new nonuniform grid schemes are stable and are able to produce highly accurate results.

Acknowledgments

This work was sponsored by AFOSR, USAF, under AFOSR Grant #F49620-00-1-0101. The views and conclusions contained herein are those of the author and should not be interpreted as necessarily representing the official policies or endorsements either expressed or implied, of AFOSR or the U.S. Government.

References

1. Zhong, X., *AIAA paper 97-0755*, 1997.
2. Zhong, X., *Journal of Computational Physics*, Vol. 144, August 1998, pp. 662–709.
3. Lele, S. K., *Journal of Computational Physics*, Vol. 103, 1992, pp. 16–42.
4. Pruett, C. D., et al., *Theoretical and Comp. Fluid Dynamics*, Vol. 7, 1995, pp. 49–76.
5. Mahesh, K., *Journal of Computational Physics*, Vol. 145, pp. 332–358, 1998.
6. Carpenter, M. H., et al., *J. of Comp. Physics*, Vol. 108, 1993, pp. 272–295.
7. Abarbanel, S. S., et al., *J. of Comp. Physics*, Vol. 160, pp. 42–66, 2000.
8. Zhong, X. and Tatineni, M., *AIAA Paper 2001-0437*, 2001.
9. Kopriva, D. A., *AIAA Journal*, Vol. 31, No. 7, 1993, pp. 1235–42.
10. Kosloff, D. and Tal-Ezer, H., *J. of Comp. Physics*, Vol. 104, pp. 457–469, 1993.
11. Zhong, X., *AIAA paper 97-0756*, January 1997.

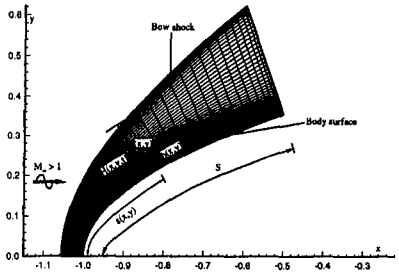

Figure 1. Computational grid for hypersonic flow over a blunt leading edge where the bow shock shape is obtained as the numerical solution for the upper grid line boundary.

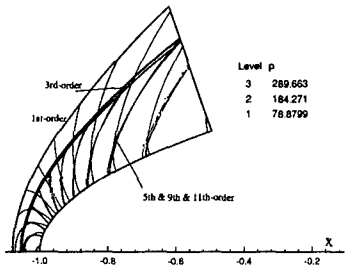

Figure 3. Pressure contours for steady base flow solutions using five nonuniform-grid schemes of the following orders: 1st, 3rd, 5th, 9th, 11th order schemes (31 × 51 grid).

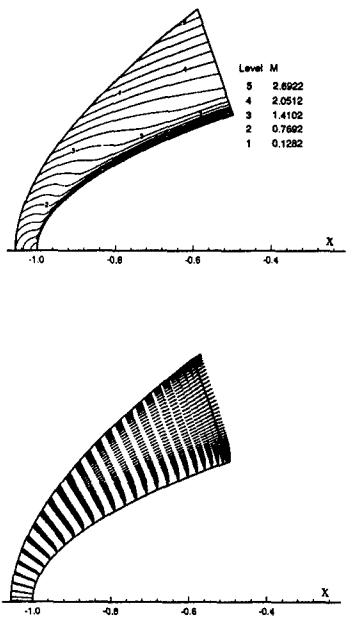

Figure 2. Mach number contours and velocity vectors for steady base flow solutions using the 11th-order nonuniform-grid scheme (31 × 51 grid).

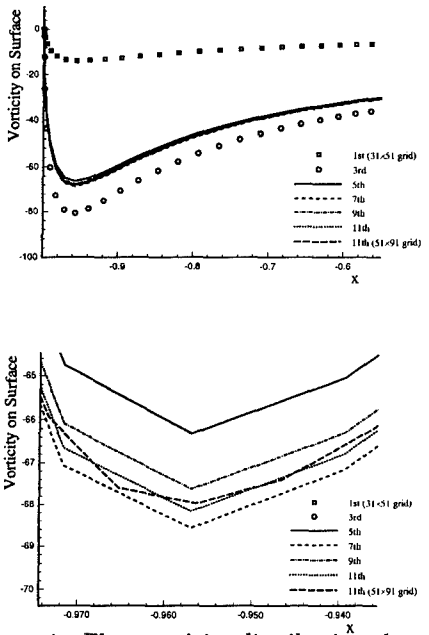

Figure 4. Flow vorticity distribution along parabola surface for steady base flow solutions using nonuniform-grid schemes of the following orders: 1st, 3rd, 5th, 9th, 11th order schemes using 31 × 51 grid and a case of 11th order using a finer grid of 51 × 91. Lower figure shows the comparison near the minimum vorticity point.

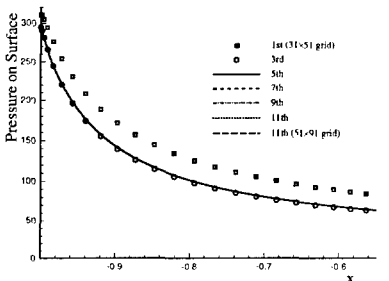

Figure 5. Stead pressure distributions along parabola surface using nonuniform-grid schemes of different orders at 31×51 and different grids.

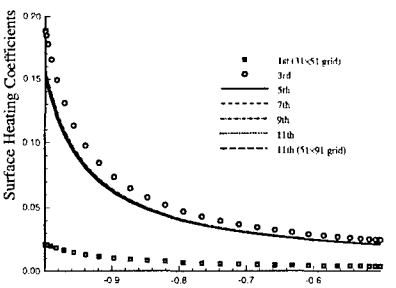

Figure 6. Nondimensional heating rates distributions along parabola surface for steady base flow solutions using nonuniform-grid schemes of different orders and different grids.

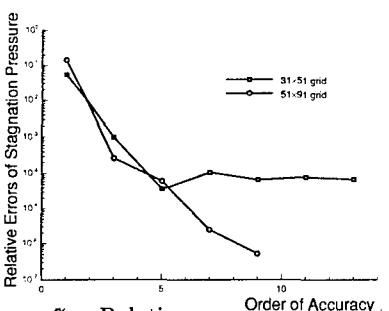

Figure 7. Relative pressure errors at the stagnation point for steady base flow solutions using nonuniform-grid schemes of different orders and different grids.

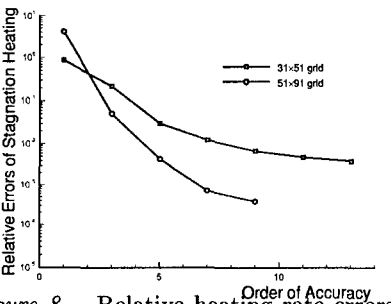

Figure 8. Relative heating rate errors at the stagnation point for steady base flow solutions using nonuniform-grid schemes of different orders and different grids.

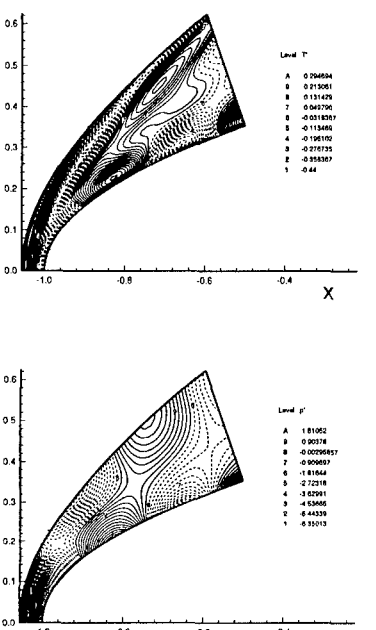

Figure 9. Instantaneous temperature and pressure perturbation contours for the case of freestream acoustic wave of $F = 2655$ and wave amplitude of 0.001. The solution is obtained by the 9th order schemes using 51×91 grid.

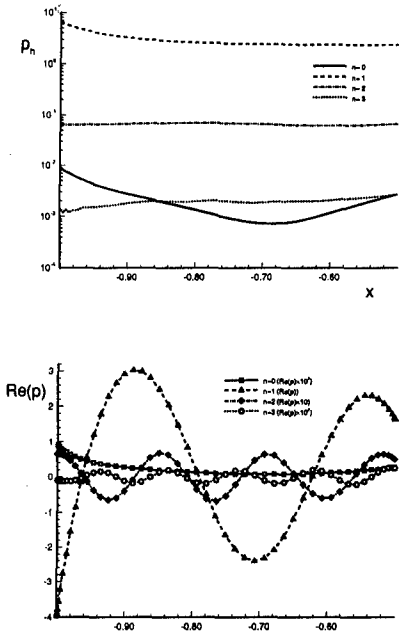

Figure 10. Fourier amplitudes of pressure perturbation and their real part along parabola surface. The solution is obtained by the 7th order schemes using 51×91 grid. In the figure, $n = 0, 1, 2, 3$, corresponds to mean flow distortion, fundamental mode, second harmonic, and third harmonic.

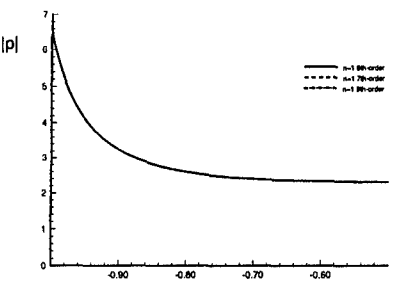

Figure 11. Fundamental mode ($\overset{x}{n} = 1$) pressure perturbation amplitudes along parabola surface. The solution is obtained by the 5th, 7th, and 9th order schemes using 51×91 grid.

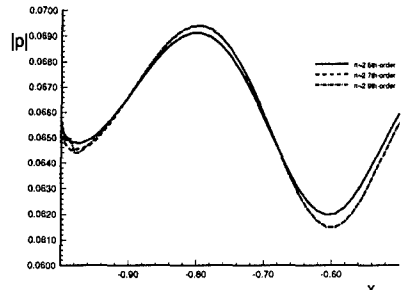

Figure 12. Second harmonic ($\overset{x}{n} = 1$) pressure perturbation amplitudes along parabola surface. The solution is obtained by the 5th, 7th, and 9th order schemes using 51×91 grid.

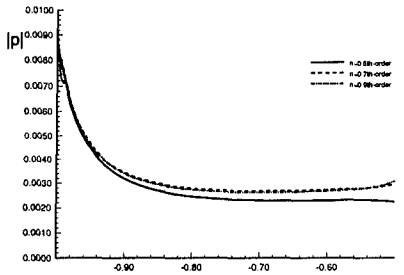

Figure 13. Mean flow distortion ($\overset{x}{n} = 0$) for pressure perturbation amplitudes along parabola surface. The solution is obtained by the 5th, 7th, and 9th order schemes using 51×91 grid.

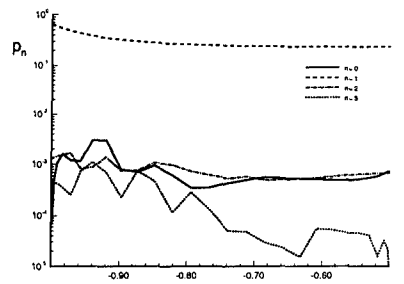

Figure 14. Fourier amplitudes pressure perturbation along parabola surface. The solution is obtained by the 9th order schemes using the coarser 31×51 grid.